Slow Photoelectron Velocity-Map Imaging of the *i*-Methylvinoxide Anion†

Tara I. Yacovitch,‡ Etienne Garand,‡ and Daniel M. Neumark*,‡,§

Department of Chemistry, University of California, Berkeley, California 94720, and Chemical Sciences Division, Lawrence Berkeley National Laboratory, Berkeley, California, 94720

Received: March 3, 2010; Revised Manuscript Received: April 19, 2010

High-resolution photoelectron spectra of the *i*-methylvinoxide anion are obtained by slow electron velocity-map imaging. The transitions between the anion ground electronic state, $\tilde{X}\ ^1A'$, and the radical $\tilde{X}\ ^2A''$, and $\tilde{A}\ ^2A'$ states are measured. Franck−Condon simulations of the $\tilde{X}\ ^2A'' \leftarrow \tilde{X}\ ^1A'$ transition are performed to aid in assigning peaks, yielding several vibrational frequencies for the first time. Additional structure in the spectrum of the $\tilde{X}\ ^2A'' \leftarrow \tilde{X}\ ^1A'$ transition is attributed to hindered rotor motion of the methyl group. Simulation of methyl torsional states allows identification of the true origin peak, yielding the experimental adiabatic electron affinity, EA = 1.747 ± 0.002 eV, and the $\tilde{A}$ state term energy, T_0 = 1.037 ± 0.002 eV. Comparison with the fully deuterated isotopologue further supports the assignment of hindered rotor progressions. The favored methyl rotor position is eclipsed in the radical $\tilde{X}$ state and staggered in the anion $\tilde{X}$ and radical $\tilde{A}$ states.

I. Introduction

Negative ion photoelectron spectroscopy (PES) yields electron affinities of atomic and molecular species as well as the changes in geometry between a negative ion and the neutral species formed by photodetachment.[1] These geometric differences appear as progressions in neutral vibrational modes, from which one can extract the changes in bond lengths and angles that occur upon photodetachment. At higher resolution, one can observe additional structure from progressions in much lower frequency internal rotations, as has been demonstrated in zero electron kinetic energy (ZEKE) spectroscopy of neutral molecules and anions,[2,3] and, more recently, in the slow electron velocity map imaging (SEVI) spectrum of the $Cl \cdot H_2^-$ anion.[4] The nature of these hindered rotor progressions provides a sensitive probe of the potential energy landscape governing molecular conformational structure. In this article, we present SEVI spectra of the *i*-methylvinoxide anion *i*-$C_3H_5O^-$ and its deuterated isotopologue. The spectra show extended hindered rotor progressions superimposed upon well-resolved vibrational structure, from which we obtain minimum energy conformations and internal rotor barrier heights for the anion and the corresponding *i*-methylvinoxy radical.

The *i*-methylvinoxy (or 1-methylvinoxy) radical *i*-C_3H_5O is a methyl-substituted vinoxy. (See Figure 1.) The associated *i*-methylvinoxide anion *i*-$C_3H_5O^-$ is also known as acetone enolate because it is the enolate form of deprotonated acetone. Like the vinoxy radical, *i*-methylvinoxy is an intermediate in combustion reactions such as that between acetone and the OH radical.[5] It is also an intermediate in organic synthetic reactions, including the industrial acetone cracking process where *i*-methylvinoxy is the species adsorbed onto a catalyzing metal surface.[6]

The *i*-$C_3H_5O^-$ anion is a closed-shell species with an $\tilde{X}\ ^1A'$ electronic ground state. Similar to the vinoxide ion, photodetachment from *i*-methylvinoxide can occur from the nonbonding $\pi(a'')$ orbital and the oxygen lone pair orbital $\sigma_{2p}(a')$,[7] yielding

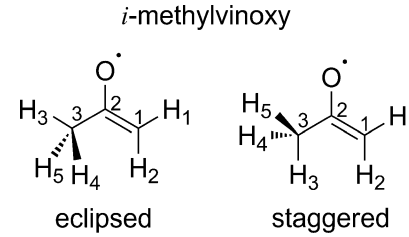

Figure 1. C_s isomers of the *i*-methylvinoxy radical.

the radical $\tilde{X}\ ^2A''$ and $\tilde{A}\ ^2A'$ states, respectively. Extensive photodetachment studies on all methylvinoxide isomers were performed by Brauman and coworkers.[8−10] This work provided an electron affinity (EA) of 1.757 ± 0.033 eV for *i*-methylvinoxy and evidence of a large geometry change between its anion and neutral. The first PE spectrum of the *i*-methylvinoxide ion was reported by Ellison et al. in 1982.[11] The spectrum accessed the $\tilde{X}\ ^2A'' \leftarrow \tilde{X}\ ^1A'$ transition and, despite broadened vibronic structure, resolved a peak at a frequency of 1100 cm^{-1} and a series of peaks spaced by ∼550 cm^{-1}. Alconcel et al.[7] reported the anion PE spectrum at higher photon energy. They observed transitions to the $\tilde{X}$ and $\tilde{A}$ radical states. Partially resolved vibrational structure within each manifold was attributed to the CCC bend in the $\tilde{A}$ state and the CC stretching motion in the $\tilde{X}$ state. This work yielded an adiabatic electron affinity (AEA) of 1.76 ± 0.02 eV and an $\tilde{A}$ state term energy of 1.01 ± 0.02 eV for *i*-methylvinoxy.

Laser induced fluorescence (LIF) studies of the *i*-methylvinoxy radical have been performed by Weisshaar and coworkers by exciting transitions to the $\tilde{B}$ state, which lies 27 282.5 ± 0.6 cm^{-1} (3.38260 ± 0.00007 eV) above the ground state.[12,13] A number of $\tilde{B}$ state backbone vibrations were identified, and considerable additional structure was attributed to hindered rotation of the methyl group. One-dimensional hindered rotor simulations were fit to experiment to yield methyl rotor barrier heights of 130 ± 30 and 740 ± 30 cm^{-1} for the $\tilde{X}$ and $\tilde{B}$ states of *i*-methylvinoxy.[13] The preferred methyl orientation was reasoned to be eclipsed for the radical $\tilde{X}$ state and staggered for the radical $\tilde{B}$ state.

† Part of the "Klaus Müller-Dethlefs Festschrift".

* Corresponding author. E-mail: dneumark@berkeley.edu.
‡ University of California.
§ Lawrence Berkeley National Laboratory.

10.1021/jp101930b © 2010 American Chemical Society
Published on Web 05/05/2010

A number of electronic structure calculations have been performed on *i*-methylvinoxy. Geometries and energies for the $\tilde{X}$ and $\tilde{B}$ states of *i*-methylvinoxy were calculated by Weisshaar and coworkers[13] and, more recently, by Yamaguchi et al.[14] Two kinetics studies reported harmonic vibrational frequencies for the $\tilde{X}$ state in their supporting information.[5,15] No frequency calculations have been reported for the *i*-C_3H_5O $\tilde{A}$ state or *i*-$C_3H_5O^-$, although results exist for the linear isomers, *n*-C_3H_5O and *n*-$C_3H_5O^-$, in both cis and trans geometries.[7,15]

In this study, we report high-resolution SEVI spectra of the *i*-methylvinoxide anion and its deuterated isotopologue. We present the first vibrational analysis of the radical $\tilde{X}$ state modes and provide more insight into the $\tilde{A}$ state transitions. Additional structure in the *i*-methylvinoxy $\tilde{X}\ ^2A'' \leftarrow \tilde{X}\ ^1A'$ transition is attributed to hindered rotor motion of the methyl substituent; no such structure is observed in the $\tilde{A}\ ^2A' \leftarrow \tilde{X}\ ^1A'$ spectrum. The most stable orientation of the methyl group is found to be eclipsed in the radical $\tilde{X}\ ^2A''$ state and staggered in both the anion $\tilde{X}\ ^1A'$ state and the radical $\tilde{A}\ ^2A'$ state. New values for the EA and $\tilde{A}$ state term energy of *i*-methylvinoxy are determined on the basis of the analysis of the methyl group hindered rotation. Franck−Condon (FC) calculations for the $\tilde{X}\ ^2A'' \leftarrow \tilde{X}\ ^1A'$ transition also aid in the assignment of vibrational modes.

II. Experimental Methods

SEVI is a high-resolution variant of negative-ion PES and has been previously described in detail.[16,17] In brief, negative ions are photodetached with a tunable laser, and the slow electrons are selectively detected using a low-voltage extraction velocity-map imaging (VMI) setup.[18] By varying the detachment wavelength, a number of high-resolution scans over limited energy windows are obtained.

The *i*-$C_3H_5O^-$ anions were produced from of a gas mixture comprising ~1% acetone in argon. Fully deuterated *i*-$C_3H_5O^-$ anions were similarly produced with an analogous gas mixture containing acetone-d_6. The gas mixture, at a stagnation pressure of 300 psi, was expanded into the source vacuum chamber through an Even−Lavie pulsed valve.[19] Anions were formed using the grid discharge source described previously,[20] then mass-selected[21] and directed to the detachment region by a series of electrostatic lenses and pinholes. They were then photodetached between the repeller and the extraction plates of the VMI assembly by the output of a Nd/YAG-pumped tunable dye laser. The resulting photoelectron cloud was coaxially extracted down a 50 cm flight tube and mapped onto a detector comprising microchannel plates coupled to a phosphor screen, as is typically used in photofragment and photoelectron imaging experiments.[22,23] Events on the screen were collected by a 1024 × 1024 charge-coupled device (CCD) camera and sent to a computer, where they were summed, quadrant-symmetrized, smoothed, and inverse-Abel transformed.[24] Photoelectron kinetic energy spectra were obtained by angular integration of the transformed images. In each SEVI image, better energy resolution was obtained for slower electrons. Therefore, by varying the photodetachment laser wavelength, a series of spectra was obtained in which different transitions were well-resolved. SEVI spectra are plotted with respect to electron binding energy (eBE), defined as the difference between the photodetachment photon energy and the measured electron kinetic energy (eKE).

The apparatus was calibrated by acquiring SEVI images of atomic O^- and S^- at several different photon energies.[25,26] With the 350 V VMI repeller voltage used in this study, a Gaussian peak width ($w = 2\sigma$) of 4.1 cm^{-1} was obtained for an atomic oxygen peak with an eKE of 33.4 cm^{-1}. Linewidths in the spectra presented in Section III were limited by unresolved asymmetric top rotational structure. Since the origin of an unresolved rotational profile may not be aligned with the observed peak maximum, we report error bars of one Gaussian standard deviation ($^1/_2\ w = \sigma$) for all energy determinations.

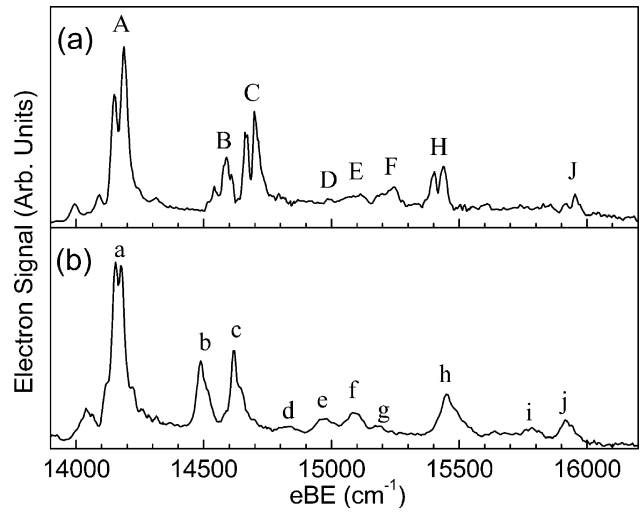

Figure 2. Composite SEVI spectra of *i*-methylvinoxide isomers (a) *i*-$C_3H_5O^-$, showing transitions to the radical $\tilde{X}\ ^2A''$ states and covering an electron binding energy range of 13 900 to 16 200 cm^{-1}. The composite spectrum is made by joining parts of spectra acquired at laser energies above threshold by (a) 2465, 1657, 946, and 410 cm^{-1} and (b) 2333, 1813, 865, and 433 cm^{-1}.

SEVI also provides information on the photoelectron angular distribution (PAD). For one-photon detachment, the PAD is given by eq 1[23]

$$\frac{d\sigma}{d\Omega} = \frac{\sigma_{total}}{4\pi}\left(1 + \beta\left(\frac{3}{2}\cos^2(\theta) - \frac{1}{2}\right)\right) \quad (1)$$

where θ is the angle between the direction of photoelectron ejection and the polarization of the incident photon. The anisotropy parameter β lies between 2 and −1 and is determined by the angular momenta of the photoelectron partial waves, which, in turn, reflect the shape of the orbital from which detachment occurs. Limiting values are $\beta = 0$ for s-wave ($l = 0$) detachment, $\beta = 2$ for p-wave ($l = 1$) detachment, and $\beta = -1$ for s+d-wave detachment. In general, the value of β depends on the detachment energy,[16] so peaks having $\beta > 1$ are simply labeled "p", whereas those with $\beta < 0.2$ or negative are labeled "s + d."

III. Results

SEVI spectra of the $\tilde{X}\ ^2A'' \leftarrow \tilde{X}\ ^1A'$ and $\tilde{A}\ ^2A' \leftarrow \tilde{X}\ ^1A'$ anion-to-radical electronic transitions of *i*-methylvinoxy and its fully deuterated isotopologue are presented in Figures 2 and 3. In each Figure, panel a shows the *i*-$C_3H_5O^-$ isotopologue with peaks labeled with uppercase letters, whereas panel b shows the *i*-$C_3D_5O^-$ isotopologue, with analogous peaks labeled in lowercase.

These spectra were constructed as follows. Several SEVI scans were taken at progressively lower photon energies to achieve high resolution for all peaks. Near each detachment energy, two or three experimental scans were averaged. The highest resolution portions of these averages were then spliced together to yield a composite spectrum with high resolution for

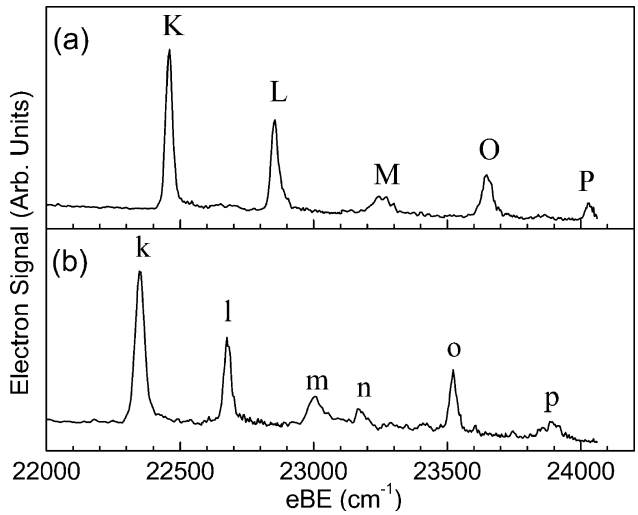

Figure 3. Composite SEVI spectra of (a) *i*-methylvinoxide isomers *i*-$C_3H_5O^-$ and (b) *i*-$C_3D_5O^-$, showing transitions to the radical $\tilde{A}\ ^2A'$ states and covering an electron binding energy range of 22 000 to 24 200 cm^{-1}. The composite spectrum is made by joining parts of spectra acquired at laser energies (a) 1637, 1407, 689, and 268 cm^{-1} above the $\tilde{A}$ state origin and (b) 1746, 1402, and 586 cm^{-1}.

all peaks. Because the relative intensity for a given peak decreases with decreasing detachment energy, each portion of the composite spectrum was also intensity scaled to match an overview SEVI spectrum taken far from threshold. The final scaled and spliced experimental spectra are shown in Figures 2 and 3. Near threshold, the Gaussian width, *w*, of most major peaks is ~25 cm^{-1}, considerably broader than atomic oxygen peaks (4 cm^{-1}) obtained under similar conditions. The broader peaks in the molecular SEVI spectra indicate that the experimental resolution is limited by the unresolved asymmetric top rotational envelope and not the instrument.

The spectra in Figures 2 and 3 show well-resolved structure dominated by the origin bands (A, a, K, and k) and followed by transitions to vibrationally excited levels of the radical $\tilde{X}$ and $\tilde{A}$ states. Several of the larger features in Figure 2, most notably A, B, C, and H, are split and show evidence of additional structure. Peak positions and assignments are summarized in Tables 1 and 2. For split peaks, the positions are given by the intensity-weighted average of the two most intense peaks. All peaks in Figure 2 have "s + d" character, whereas those in Figure 3 have "p" character, indicating photodetachment transitions to two distinct electronic states. The main additional features of the *i*-C_3H_5O $\tilde{X}$ state spectrum (Figure 2a) are peaks B, C, and H, which occur at 401, 515, and 1247 cm^{-1} from the main peak A. The deuterated spectrum in Figure 2b shows similar vibrational structure, with slight differences in frequencies for most peaks and different intensities for peaks d−f and j. The $\tilde{A}$ state spectrum in Figure 3a is characterized by a progression of peaks K, L, and M spaced by 395 and 399 cm^{-1}, with peaks O and P appearing at frequencies of 1191 and 1573 cm^{-1} from peak K. The deuterated spectrum in Figure 3b shows similar structure with an additional peak, labeled n, appearing at 823 cm^{-1} higher energy than peak k. The spectra in Figures 2 and 3 show significantly more structure than the previous PE spectra of Ellison et al.[11] and Alconcel et al.[7]

IV. Analysis

1. Electronic Structure Calculations. Geometry optimizations and frequency calculations were performed on the ground states of the *i*-methylvinoxide anion and the corresponding radical. Density functional theory (DFT) was chosen for the purpose of this study because it balances acceptable accuracy with a low computational load. The B3LYP functional was used with the 6-311++G** basis set. All frequencies were scaled by a factor of 0.9679, as is standard for B3LYP calculations with Pople-style basis sets.[27] The Gaussian 03 suite of programs[28] was used throughout.

The molecular symmetry was restricted to the C_s point group, consistent with previous studies on the *i*-methylvinoxy isomers.[13] Within this point group, two conformational isomers corresponding to different methyl group orientations are possible, as shown in Figure 1. In the "staggered" (or "eclipsed") conformer, the in-plane methyl hydrogen H(3) is at a dihedral angle of 180° (or 0°) from the oxygen atom in *i*-methylvinoxy.

Table 3 lists calculated geometries for the $\tilde{X}$ states of *i*-$C_3H_5O^-$ and *i*-C_3H_5O. Our calculations found the lowest-energy anion structure to be staggered and the lowest-energy radical structure to be eclipsed. The radical backbone geometries are within 0.02 Å of previous calculations (included in Table 3) at the (5,4)-CASSCF/6-31G(d,p) level of theory.[13] The staggered radical structure is also shown for comparison because it was used in the FC simulations discussed in Section IV.2.A.

Experimentally relevant scaled frequencies for the anion and radical $\tilde{X}$ states are shown in Table 4 along with their normal mode descriptions. Values for the deuterated species are also included. The vibrational frequencies in the anion and radical $\tilde{X}$ state are generally similar, and within each symmetry (a′ or a″) are ordered according to their value in the *i*-C_3H_5O eclipsed radical $\tilde{X}$ state. The large conformational change between the anion (staggered) and the $\tilde{X}$ state radical (eclipsed) leads us to expect extended vibrational progressions in the methyl torsional mode, ν_{21}. However, the low frequency of this mode, particularly in the neutral (30 cm^{-1}), indicates that it is better treated as a hindered rotation than a torsional vibration. Note that the calculated frequency for this mode is imaginary for the staggered geometry of the radical, as expected.

The minimum energy geometries in Table 3 were used as a starting point for methyl rotor barrier calculations. The H(3)C(3)C(2)O dihedral angle in the anion and radical was scanned at the same level of theory, keeping all other coordinates constant. This yields a potential surface with three minima and maxima but with imperfect three-fold symmetry due to the distortions in the methyl group geometry in the converged C_s equilibrium structure. A radical barrier height of 123 cm^{-1} and an anion barrier height of 890 cm^{-1} can be extracted by taking the difference in energies of conformers with H(3)C(3)C(2)O dihedral angles of 180 and 0° (staggered and eclipsed). These energy values do not include zero-point corrections and are thus valid for the deuterated species as well. When all coordinates except the dihedral angle are allowed to relax during the hindered rotor scan, three-fold symmetry is recovered, and lower barrier heights are obtained (25 and 700 cm^{-1} for the radical and anion, respectively). Compared with the rigid scan results, these relaxed scans show an increase in both C(2)C(3) bond length and H(3)C(3)C(2) bond angle at the top of the rotor wells, effectively moving the methyl group away from the rest of the structure. Hindered rotor calculations based on these calculated potentials are described in Section IV.2.B.

2. Simulations. FC simulations of the ground-state *i*-methylvinoxy system are complicated by the need to simulate both vibrational and hindered rotor motion. For this system, the total nuclear wave function Ψ can be decomposed into a product of vibrational (ψ_v) and hindered rotor (ψ_m) wave functions, where ψ_v itself is a product of multiple vibrational wave functions.

TABLE 1: Experimental Peak Positions, Vibrational Frequencies, and Assignments of Vibrational Transitions in the $\tilde{X}\ ^2A''$ Electronic State of the *i*-Methylvinoxy Radical

i-C_3H_5O $\tilde{X}\ ^2A''$			*i*-C_3D_5O $\tilde{X}\ ^2A''$			
label[a]	position (cm^{-1})	vibrational frequency (cm^{-1})	label[a]	position (cm^{-1})	vibrational frequency (cm^{-1})	assignment[c]
A	14 172[b]	0	a	14 164[b]	0	0−0
B	14 573[b]	401	b	14 492[b]	328	14_0^1
C	14 687[b]	515	c	14 626[b]	462	13_0^1
D	14 992	820	d	14 854	690	14_0^2?
E	15 112	939	e	14 972	808	$13_0^1\ 14_0^1$
F	15 220[b]	1048	f	15 087	922	13_0^2
			g	15 178	1014	7_0^1?
H	15 410[b]	1247	h	15 423[b]	1259	9_0^1
			i	15 782	1618	$9_0^1\ 14_0^1$
J	15 940[b]	1767	j	15 921	1756	$9_0^1\ 13_0^1$

[a] Peak labels refer to Figure 2. [b] Positions of split peaks are given by intensity-weighted averages of the two major subpeaks. [c] See Table 4 for normal mode descriptions.

TABLE 2: Experimental Peak Positions, Vibrational Frequencies, and Assignments for the $\tilde{A}\ ^2A'$ Electronic State of the *i*-Methylvinoxy Radical

i-C_3H_5O $\tilde{A}\ ^2A'$			*i*-C_3D_5O $\tilde{A}\ ^2A'$			
label[a]	position (cm^{-1})	shift (cm^{-1})	label[a]	position (cm^{-1})	shift (cm^{-1})	assignment[b]
K	22 460	0	k	22 350	0	0−0
L	22 854	395	l	22 677	327	14_0^1
M	23 253	794	m	23 006	656	14_0^2
			n	23 174	823	$13_0^1\ 14_0^1$?
O	23 650	1191	o	23 522	1172	9_0^1
P	24 032	1573	p	23 887	1536	$9_0^1\ 14_0^1$

[a] Peak labels refer to Figure 3. [b] See Table 4 for normal mode descriptions.

TABLE 3: Calculated Geometries for the *i*-Methylvinoxide Anion *i*-$C_3H_5O^-$ and the *i*-C_3H_5O Radical Using Density Functional Theory, the B3LYP Functional, and the 6-311++G Basis Set[a]**

	anion $\tilde{X}$	radical $\tilde{X}$		
	staggered	staggered[b]	eclipsed	eclipsed[c]
Bond Length (Å)				
C(1)C(2)	1.386	1.435	1.439	1.451
C(2)C(3)	1.547	1.519	1.519	1.514
OC(2)	1.272	1.238	1.235	1.221
H(1)C(1)	1.086	1.083	1.083	
H(2)C(2)	1.085	1.083	1.084	
H(3)C(3)	1.096	1.091	1.089	
H(4)C(3)	1.097	1.093	1.094	
H(5)C(3)	1.097	1.093	1.094	
Angles (Degrees)				
C(1)C(2)C(3)	116.9	119.7	118.4	118.7
OC(2)C(1)	127.8	120.1	120.3	120.2
H(1)C(1)C(2)	120.2	118.5	118.7	
H(2)C(1)C(2)	121.6	122.2	122.0	
H(3)C(3)C(2)	113.5	113.1	109.9	
H(4)C(3)C(2)	109.1	109.1	110.6	
H(5)C(3)C(2)	109.1	109.1	110.6	
Dihedral Angles (degrees)				
H(3)C(3)C(2)C(1)	180.0	180.0	0.0	
H(4)C(3)C(2)C(1)	−121.7	−121.6	59.4	
H(5)C(3)C(2)C(1)	121.7	121.6	−59.4	

[a] Atom labels refer to Figure 1. [b] Nonequilibrium staggered radical geometry used in Franck−Condon simulations. (See Section IV.2.A.) [c] (5,4)-CASSCF/6-31G(d,p) in ref 13.

The hindered rotation of the methyl group is assumed to be sufficiently decoupled from all other vibrational motions that the coordinates of ψ_v and ψ_m are effectively independent. This allows for the separation of the total FC factor into a product of vibrational (FC_{vib}) and hindered rotor (FC_{CH_3rot}) parts, where line intensities are proportional to FC factors for the overlap of the anion states, $\psi_{v'}\psi_{m'}$ with the radical states, $\psi_{v''}\psi_{m''}$ (eq 2).

$$FC_{total} = |\langle\psi_{v''}\psi_{m''}|\psi_{v'}\psi_{m'}\rangle|^2 = |\langle\psi_{v''}|\psi_{v'}\rangle\langle\psi_{m''}|\psi_{m'}\rangle|^2 = FC_{vib}FC_{CH_3rot} \quad (2)$$

We treat the vibrational FC simulations in Section IV.2.A, and the hindered rotor FC simulations in Section IV.2.B.

A. Vibrational Franck−Condon Simulations. Vibrational FC simulations were performed on the $\tilde{X}\ ^2A'' \leftarrow \tilde{X}\ ^1A'$ transition. Vibrational line intensities are proportional to FC_{vib} factors for the overlap of the anion's lowest vibrational level, $\psi_{v'}$, with the vibrational levels in the radical, $\psi_{v''}$ (eq 2). The Born−Oppenheimer principle is assumed as well as a constant electronic transition moment. The initial ($\boldsymbol{Q}$) and final ($\boldsymbol{Q'}$) normal coordinates are related by the Duschinsky transformation[29] (eq 3).

$$\boldsymbol{Q} = \mathbf{J}\boldsymbol{Q'} + \mathbf{K} \quad (3)$$

Here **J** is the Duschinsky rotation matrix, which represents the mixing of normal modes. It is block diagonal for modes of the same symmetry. **K** is the normal coordinate displacement vector that expresses the difference between the neutral and anion equilibrium geometries in terms of the neutral normal coordinates.

In the course of the following calculations, we will assume that the normal mode corresponding to methyl torsion is an independent harmonic oscillator with no Duschinsky mixing with other modes. The methyl torsion will then be treated as a hindered rotation in Section IV.2.B. A similar treatment has been used to study other systems.[30,31] Mathematically, this is equivalent to assuming that there are no off-diagonal terms for the **J** matrix element corresponding to methyl torsion. This

TABLE 4: Selected Normal Modes and Scaled Vibrational Frequencies of the *i*-Methylvinoxide Anion, *i*-Methylvinoxy Radical, and Isotopologues Calculated at the B3LYP/6-311++G Level of Theory**

			anion $\tilde{X}\ ^1A'$		radical $\tilde{X}\ ^2A''$						radical $\tilde{A}\ ^2A'$	
			i-$C_3H_5O^-$	*i*-$C_3D_5O^-$	*i*-C_3H_5O			*i*-C_3D_5O			*i*-C_3H_5O	*i*-C_3D_5O
mode[a]	description (approximate)[b]	sym	calcd staggered	calcd staggered	calcd eclipsed	calcd staggered[c]	exptl	calcd eclipsed	calcd staggered[c]	exptl	exptl	exptl
ν_5	CO stretch and CCC symmetric stretch	a′	1528	1499	1532	1501		1483	1492			
ν_7	CH_2 bend and CH_3 umbrella	a′	1397	985	1409	1414		1066	1002	1014		
ν_9	CCC asymmetric stretch	a′	1243	985	1226	1222	1247	1187	1251	1259	1191	1172
ν_{13}	OCC bend	a′	495	441	510	501	515	494	450	462		497
ν_{14}	CCC bend	a′	409	344	375	392	401	363	329	328	395	327
ν_{21}	methyl torsion	a″	169	122	30	37*i*		29	27*i*			

[a] Normal modes are numbered according to their value in the ground-state *i*-C_3H_5O radical. [b] Atom labels refer to Figure 1. [c] Radical frequencies calculated at the nonequilibrium staggered conformation are used in Franck−Condon simulations. (See Section IV.2.A.)

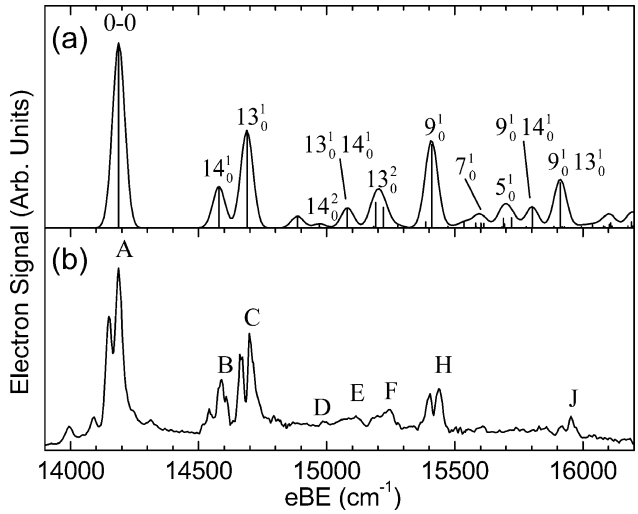

Figure 4. Vibrational Franck−Condon simulation of the $\tilde{X}\ ^2A'' \leftarrow \tilde{X}\ ^1A'$ transition in *i*-C_3H_5O. The simulation in panel a is shown above the experimental composite spectrum in panel b. The labels in panel a refer to the normal modes described in Table 4.

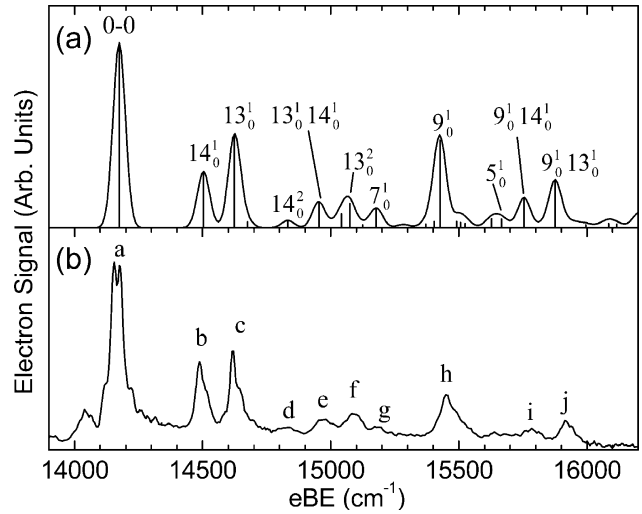

Figure 5. Vibrational Franck−Condon simulation of the $\tilde{X}\ ^2A'' \leftarrow \tilde{X}\ ^1A'$ transition in *i*-C_3D_5O. The simulation in panel a is shown above the experimental composite spectrum in panel b. The labels in panel a refer to the normal modes described in Table 4.

assumption is reasonable because the a″ torsional mode, by symmetry, will have no Duschinsky mixing with the a′ modes, which are the main contributors to the simulated spectrum. Using the set of programs prepared by Ervin and coworkers, the **J** matrix and **K** vector for all vibrations are computed in FCFGAUS,[32] and then all modes except for methyl torsion are treated with Duschinsky rotation in Pescal.[33] In keeping with our assumed separation of vibrational and internal rotor degrees of freedom, the optimized staggered conformations for the anion and neutral were used in calculating FC_{vib}. Using these geometries eliminates complications that arise when attempting to compare normal modes in two species with significant structural differences[34] yet allows the backbone vibrations to be simulated with reasonable accuracy.

FC_{vib} simulations at 0 K are shown in Figures 4a and 5a for *i*-C_3H_5O and *i*-C_3D_5O, respectively. These simulations reproduce the major features of the experimental spectra shown in Figures 4b and 5b, except for the splitting and finer structure that is visible for most intense peaks. Assignments of the main vibrational features of the $\tilde{X}\ ^2A'' \leftarrow \tilde{X}\ ^1A'$ transition are made based on these results and shown in Table 1.

B. Hindered Internal Rotor Simulations. The 1D hindered rotor model is used to calculate transition energies and intensities from the $\tilde{X}\ ^1A'$ state of *i*-methylvinoxide to the $\tilde{X}\ ^2A''$ state of *i*-methylvinoxy. Detailed derivations of the treatment, outlined below, can be found in the series of papers by Pitzer.[35−37]

The equilibrium C_s structures (staggered anion and eclipsed radical) were used in the calculation of rotational constants. (See Section IV.1.) First, the reduced moment of inertia for the methyl top is calculated from eq 4

$$I_{CH_3} = I_{CH_3}\left[1 - I_{CH_3}\left(\frac{\lambda_a^2}{I_a} + \frac{\lambda_b^2}{I_b} + \frac{\lambda_c^2}{I_c}\right)\right] \qquad (4)$$

which involves the three principal moments of inertia of the equilibrium molecule (I_n), the moment of inertia of the methyl top about its rotational axis (I_{CH_3}), and the angles between them in the form of direction cosines. Denoted λ_n, the direction cosine is the dot product between unit vectors representing the methyl rotor axis, $\vec{v}_{rot}$, and the principal inertial axis, *n*, of the equilibrium molecule

$$\lambda_n = |\vec{v}_{rot} \cdot \vec{I}_n| \qquad (5)$$

The reduced rotational constant of the methyl rotation (B_{CH_3}) is given by

$$B_{CH_3} = \frac{\hbar^2}{2I_{CH_3}} \tag{6}$$

A torsional potential for methyl rotation, $V(\phi)$, can be expanded in terms of V_3 and V_6 potential terms where the dihedral angle ϕ is the angle between the CO bond and one of the methyl CH bonds.

$$V(\phi) = \frac{V_3}{2}(1 - \cos 3\phi) + \frac{V_6}{2}(1 - \cos 6\phi) + ... \tag{7}$$

The *i*-methylvinoxy ground-state radical is most stable in its eclipsed form, with potential minima at H(3)CCO dihedral angles of $\phi = 0$, 120, and 240°, whereas the *i*-methylvinoxide anion is most stable in its staggered form ($V_3 < 0$) with potential minima shifted by 60°. The potential energy scans in Section IV.1 showed no signs of significant contribution of the V_6 potential term.

The relevant Hamiltonian for the rigid rotor problem is

$$H(\phi) = -B_{CH_3}\frac{\partial^2}{\partial\phi^2} + V(\phi) \tag{8}$$

The wave function is expanded in a basis of 81 free-rotor functions ($\Phi_m(\phi) = e^{im\phi}$) allowing the Hamiltonian matrix elements to be evaluated directly

$$H_{m'',m'}(\phi) = \left(B_{CH_3}(m')^2 + \frac{V_3}{2}\right)\delta_{m'',m'} - \frac{V_3}{4}\delta_{m'',m'\pm 3} - ... \tag{9}$$

The eigenvalue problem was solved, yielding rotational energy levels and wave functions with a_1, a_2, and e (doubly degenerate) symmetries. Figure 6 shows the *i*-C_3H_5O and *i*-$C_3H_5O^-$ hindered rotor wells used in the calculation along with the simulated energy levels. Levels are numbered according to convention: $0a_1$, $1e$, $2e$, $3a_2$, $3a_1$, $4e$, $5e$, $6a_2$, $6a_1$, $7e$, $8e$, $9a_2$, $9a_1$, ... Hindered rotor Franck−Condon factors (FC_{CH_3rot}) between levels were then calculated from eq 2. These FC_{CH_3rot} intensities are combined with Boltzmann factors for our expected temperature of 70 K, taking into account the doubly degenerate states. This temperature is a reasonable estimate based on the absence of significant hotbands in the experimental spectra. At 70 K and considering the depth of the anion well (Figure 6), the majority of the population resides in the essentially degenerate $0a_1$ and $1e$ states. Nuclear spin statistics must also be considered. Following the treatment of Bunker and Jensen,[38] all rovibronic levels are equally weighted for a CH_3 rotor and with ratios of 0.69:0.69:1.0 for a CD_3 rotor. Finally, because the simulations aim to reproduce experimental data taken very close to threshold, a pure "s-wave" character with $l = 0$ is assumed, and the simulated line intensities weighted according to the Wigner threshold law, $eKE^{l+0.5}$.[39]

Hindered rotor simulations for the *i*-C_3H_5O and *i*-C_3D_5O systems are shown in Figures 7a and 8a, respectively, using $V_3 = 123$ cm^{-1} for the radical and -890 cm^{-1} for the anion. These were the barrier heights obtained from the one-dimensional rigid scan calculations in Section IV.1, which describe a 1D hindered rotor fully decoupled from any vibrational motion like C(2)C(3) stretching. The relaxed scan barriers performed extremely poorly

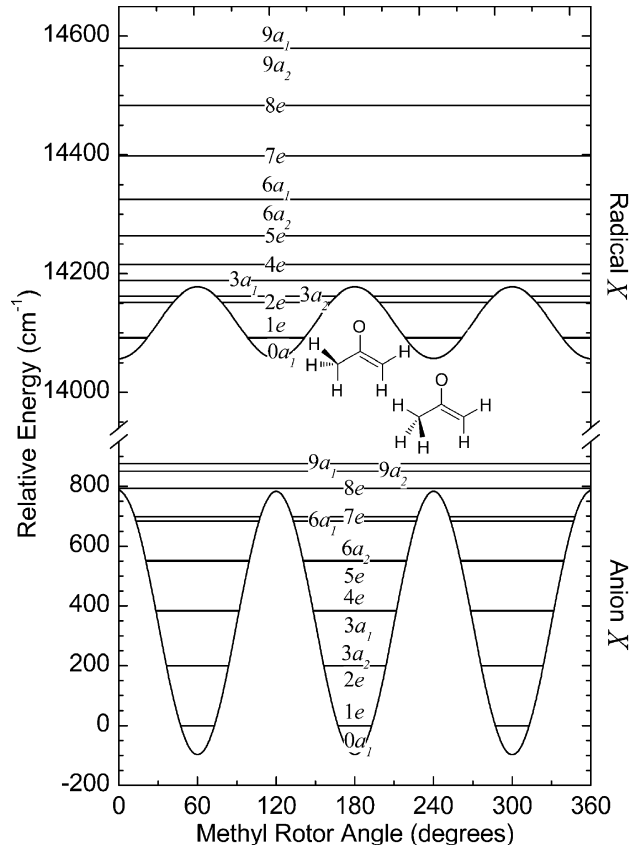

Figure 6. Hindered rotor energy levels and potentials (from eq 7) for the anion $\tilde{X}\ ^1A'$ state and the radical $\tilde{X}\ ^2A''$ state of *i*-C_3H_5O. Energy levels are numbered according to convention and labeled with their symmetries (a_1, a_2, and e). Methyl rotor angles of 0, 120, or 240° correspond to eclipsed geometries, whereas methyl rotor angles of 60, 180, or 300° correspond to staggered geometries.

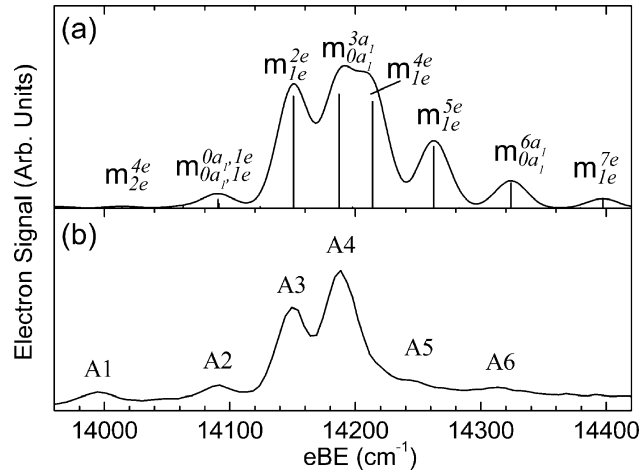

Figure 7. Hindered rotor splitting for the *i*-C_3H_5O radical. (a) Results from hindered rotor simulations using the equilibrium geometries in Table 3 and barrier heights V_3 in Table 6. A Gaussian convolution of the line spectrum at $w = 25$ cm^{-1} is also shown. (b) Experimental spectrum.

and are not presented here. As described in Section IV.1, the relaxed scans showed changes in C(2)C(3) bond length and H(3)C(3)C(2) bond angle during methyl rotation, destroying the "1D" nature of the rotation. It is perhaps reasonable then that these multidimensional barrier heights are inappropriate for the 1D calculations described in this section.

The simulations were translated to best match the experimental scans, shown in Figures 7b and 8b. This is equivalent

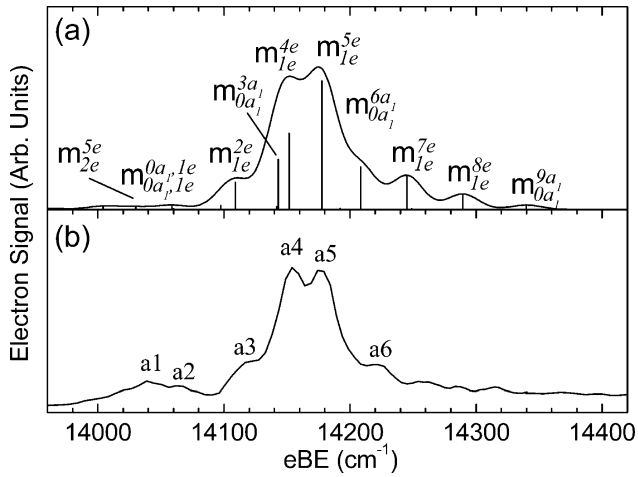

Figure 8. Hindered rotor splitting for the *i*-C_3D_5O radical. (a) Results from hindered rotor simulations using the equilibrium geometries in Table 3 and barrier heights V_3 in Table 6. A Gaussian convolution of the line spectrum at $w = 25$ cm^{-1} is also shown. (b) Experimental spectrum.

to adding a constant potential energy offset between the radical and anion (Figure 6) and does not change the resulting peak spacings or intensities. The simulated features are labeled m_l^f to indicate transitions between the initial hindered rotor state in the anion and the final hindered rotor state in the radical. Only transitions between levels of the same symmetry are allowed. Experimental assignments based on these simulations are reported in Table 5. The first two hindered rotor levels, $0a_1$ and $1e$, are so close in energy (0.80 cm^{-1} in the *i*-C_3H_5O radical, for example) that they appear as a single peak in the simulations; this is the true 0−0 transition in eq 2. Note that the 0−0 transition is rather weak for both isotopologues.

By testing the effect of different simulated potential values, we are able to estimate approximate error bars of 15 cm^{-1} in either direction for the radical barrier height; beyond these limits, peak assignments, and the resulting EA begins to change. The error estimate for the anion barrier height (∼400 cm^{-1} or more) is significantly larger because only the lowest levels ($0a_1$ and $1e$) of the deeper anion well are populated.

V. Discussion

Results of the FC_{vib} simulations in Figures 4 and 5 and internal rotor simulations in Figures 7 and 8 were used to make assignments for the $\tilde{X}$ state spectra discussed in Section IV.1 below and reported in Tables 1 and 2. The $\tilde{A}$ state spectra are significantly simpler than the ground state spectra, and it is possible to assign most transitions convincingly simply by comparison with the $\tilde{X}$ state spectra. (See Section V.2 and Table 4.) All normal modes in Tables 1, 2, and 4 are numbered according to their value in the $\tilde{X}$ state *i*-C_3H_5O radical. The notation v_n^m is used throughout, to indicate transitions in the v vibrational mode with n quanta in the anion and m quanta in the neutral.

1. $\tilde{X}$ State. The splittings of the major peaks in the $\tilde{X}$ state spectrum indicate that the anion and radical ground state have different methyl group orientations. This observation agrees with the electronic structure calculations presented in Section IV.1 that predict a staggered conformation for the anion and an eclipsed conformation for the radical $\tilde{X}$ state. Weisshaar and coworkers also predict an eclipsed geometry for the radical $\tilde{X}$ state,[12,13] and were able to simulate the $\tilde{B} \leftarrow \tilde{X}$ LIF spectrum with the same 1D rotor model used here. They found that the methyl group orientation switches between $\tilde{B}$ and $\tilde{X}$ states and, based on calculations, determined that the $\tilde{X}$ state is in an eclipsed conformation. Experimental hot bands allowed them to fit the $\tilde{X}$ state rotational barrier to a value of 130 ± 30 cm^{-1}. This value is close to the value of 123 cm^{-1} used to simulate the spectra in Figures 7 and 8.

The $m_{0a_1,1e}^{0a_1,1e}$ transition in Figure 7a is assigned to the experimental peak A2 at 14 090 cm^{-1}. The $m_{0a_1,1e}^{0a_1,1e}$ transition in Figure 8a appears at position a2 with a simulated relative intensity of only ∼1%; we should thus not expect a clear experimental peak at this binding energy. A bump in the baseline is barely visible in the composite experimental trace at position a2 at 14 060 cm^{-1}. The two most prominent simulated peaks in the *i*-C_3H_5O spectrum in Figure 7 are m_{1e}^{2e} and $m_{0a_1}^{3a_1}$, corresponding to the experimental A3 and A4 transitions. The *i*-C_3D_5O spectrum in Figure 8 shows two intense peaks, a4 and a5, due to $m_{0a_1}^{3a_1}$ and m_{1e}^{4e} (which overlap) and m_{1e}^{5e}. Other assigned transitions appear in Table 5.

At higher eBE, the simulated transitions do not agree as well with experiment. For example, peak m_{1e}^{4e} in Figure 7a and peak m_{1e}^{7e} in Figure 8a differ from the experimental spectrum. In previous simulations of this type,[13] an additional intensity fitting of the spectrum was achieved through empirically scaling the first peak of each symmetry, a_1, a_2 and e, to experiment. We have kept the original simulated intensities in our results, but note that this type of empirical scaling would decrease the intensity of all of the e peaks that account for the major discrepancies in the *i*-C_3H_5O simulation. These discrepancies could also arise from the breakdown of the 1D hindered rotor model at higher energies, caused, for example, by coupling of the rotor motion to other low-frequency vibrations. An overestimation of the rotational constants would also give more widely spaced peaks, contributing to errors in simulated peak position.

The main vibrational features in the $\tilde{X}\ ^2A'' \leftarrow \tilde{X}\ ^1A'$ spectra (Figure 2) are from bending and stretching motions of the carbon−oxygen backbone. Features B and D are assigned to the 14_0^1 and 14_0^2 transitions of the ν_{14} CCC bending mode. Peaks C and F constitute a progression of the other backbone bending mode, the ν_{13} OCC bend. These bending vibrations have experimental frequencies of 515 and 401 cm^{-1}, respectively, for ν_{13} and ν_{14}. The analogous vibrations in the deuterated compound have frequencies of 462 and 328 cm^{-1}. Scaled frequencies calculated at the B3LYP/6-311++G** level yield bending frequencies for ν_{13} and ν_{14} of 510 and 375 cm^{-1} for *i*-C_3H_5O; 494 and 363 cm^{-1} for *i*-C_3D_5O. These values are in good agreement with experiment. The OCC bend ν_{13} of *i*-C_3H_5O is also similar to the OCC bend in the vinoxy radical, $\nu_9 = 498$ cm^{-1}, as determined by previous experiments.[40,41] Peak H is the other major transition in the ground-state spectrum. It is assigned to the ν_9 CCC asymmetric stretching mode, which occurs at a frequency of 1247 cm^{-1} in *i*-C_3H_5O and 1259 cm^{-1} in *i*-C_3D_5O. This normal mode is similar to the ν_7 CC stretch in the vinoxy radical, for which the frequency is 1137 cm^{-1}.[40,42]

The remaining peaks are mostly combination bands of the previous three backbone modes. Peaks E and J and the corresponding transitions in the deuterated spectrum (e and j) correspond to the $13_0^1 14_0^1$ and $9_0^1 13_0^1$ combination bands, respectively. Peaks g and i, which only appear with significant intensity in the deuterated spectrum, are assigned to the 7_0^1 CH_2 bending mode and the $9_0^1 14_0^1$ combination band. There is some uncertainty to the validity of this assignment because the ν_7 normal mode also contains an umbrella-like motion of the methyl hydrogens. The FC simulation also predicts a peak due

TABLE 5: Hindered Rotor Splitting in the Origin Peaks of the $\tilde{X}\ ^2A''$ Electronic State of the *i*-Methylvinoxy Radical

i-C_3H_5O $\tilde{X}\ ^2A''$			*i*-C_3D_5O $\tilde{X}\ ^2A''$		
label[a]	position (cm^{-1})	hindered rotor transition	label[a]	position (cm^{-1})	hindered rotor transition
A1	13 996	m_{2e}^{4e}	a1	14 045	m_{2e}^{5e}
A2	14 091	$m_{0a_1;1e}^{0a_1;1e}$	a2	14 060	$m_{0a_1;1e}^{0a_1;1e}$
A3	14 151	m_{1e}^{2e}	a3	14 119	m_{1e}^{2e}
A4	14 188	$m_{0a_1}^{3a_1}(m_{1e}^{4e})$	a4	14 154	$m_{0a_1;1e}^{3a_1;4e}$
A5	14 243	m_{1e}^{5e}	a5	14 175	m_{1e}^{5e}
A6	14 310	$m_{0a_1}^{6a_1}$	a6	14 219	m_{1e}^{7e}

[a] Peak labels refer to Figures 7 and 8.

to ν_5, a normal mode comprising CO stretching, and CCC symmetric stretching mode, which would appear between peaks H and J (h and i), but the 5_0^1 peak does not appear in the experimental spectrum.

The previous experimental spectra showing the $\tilde{X}\ ^2A'' \leftarrow \tilde{X}\ ^1A'$ photodetachment transition are extremely convoluted, and although some structure is visible in the PE spectra of Ellison et al.[11] and in the electron photodetachment results of Brauman and coworkers,[8,9] no clear assignment of specific $\tilde{X}\ ^2A'' \leftarrow \tilde{X}\ ^1A'$ vibrational transitions was made. Additionally, no previous frequency calculations specific to the ground-state *i*-C_3H_5O radical have been reported. This study thus represents the first systematic analysis of the vibrations in the $\tilde{X}$ state of *i*-methylvinoxy.

2. $\tilde{A}$ State. Peaks in the $\tilde{A}$ state spectrum display no visible splitting, Hence, it appears that the lowest energy structure of the $\tilde{A}$ state radical is a staggered conformation, such that transitions from the anion (also in a staggered conformation, and with a relatively deep rotor well) do not cause transitions to excited hindered rotor states. We cannot say much about the barrier to hindered rotation in the $\tilde{A}$ state; as long as the conformation is the same as the anion, there will be no pronounced hindered rotor progression.

The simplicity of the radical $\tilde{A}$ state SEVI spectrum facilitates assignments based solely on comparison with the $\tilde{X}$ state of *i*-methylvinoxy. In Figure 3, peaks K, L, and M (k, l and m) form a progression of peaks spaced by around 395 cm^{-1} (327 cm^{-1} for *i*-$C_3D_5O^-$). We assign them to a progression in the CCC bending mode, ν_{14}, analogously to the $\tilde{X}$ state spectrum. (See Tables 2 and 4.) This assignment is in agreement with previous PES experiments, which found a CCC or CCO bending frequency of 400 cm^{-1}.[7] Peaks O and o at 1191 and 1172 cm^{-1} in the *i*-C_3H_5O and *i*-C_3D_5O spectra, respectively, are assigned to the 9_0^1 transitions involving the CCC asymmetric stretching mode, which has a similar frequency in the $\tilde{X}$ state. Peaks P and p can be assigned to a combination band between the CCC asymmetric stretch and CCC bend: $9_0^1\,14_0^1$. The previous PES results assigned this transition (a frequency of 1700 cm^{-1}) to the CC stretching mode,[7] but we believe that our assignment is preferable.

The remaining peak, n, which appears only in the deuterated spectrum, is tentatively assigned to the $13_0^1\,14_0^1$ combination band involving the OCC and CCC bending vibrations. This assignment yields a value of 497 cm^{-1} for the ν_{13} vibration in the deuterated $\tilde{A}$ state, very similar to the value of ν_{13} in the $\tilde{X}$ state radical (494 cm^{-1}). A weak peak for the fundamental 13_0^1 transition should then be expected at binding energies of 22 847 cm^{-1} between peaks l and m. No clear peak is seen, but lower resolution scans show some weak, unresolved structure at this position, which disappears for the higher resolution scans in Figure 3. A similar $13_0^1\,14_0^1$ transition might be expected around 910 cm^{-1} in the *i*-C_3H_5O spectrum, assuming that an $\tilde{A}$ state ν_{13} frequency equal to the $\tilde{X}$ state ν_{13} frequency (515 cm^{-1}) combines with the $\tilde{A}$ state ν_{14} mode (395 cm^{-1}). This could account for the tail end of peak M in Figure 3a. Alternatively, peak n may be a υ_0^2 transition in a non-totally symmetric mode, which changes substantially in frequency between the anion and the radical $\tilde{A}$ state.

TABLE 6: Experimental Adiabatic Electron Affinities (AEAs), Vertical Electron Affinities[a] (vEAs), and Term Energies (T_0) along with Calculated Hindered Methyl Rotor Barriers[b] (V_3) and Rotational Constants[c] (B_{CH_3}) for $\tilde{X}$ *i*-Methylvinoxide and $\tilde{X}$ *i*-Methylvinoxy

	i-C_3H_5O	*i*-C_3D_5O
EA	1.747 ± 0.002 eV	1.743 ± 0.002 eV
vEA[a]	1.759 ± 0.002 eV	1.755 ± 0.002 eV
T_0	1.037 ± 0.002 eV	1.028 ± 0.002 eV
	$\tilde{X}$ Anion	
V_3	−890 ± 400 cm^{-1}	−890 ± 400 cm^{-1}
B_{CH_3}	5.66 cm^{-1}	2.97 cm^{-1}
	$\tilde{X}$ Radical	
V_3	123 ± 15 cm^{-1}	123 ± 15 cm^{-1}
B_{CH_3}	5.699 cm^{-1}	3.005 cm^{-1}

[a] Position of the most intense origin peak. See Section V.3 of the text. [b] Rotor barriers are calculated with a rigid scan of the H(3)CCO dihedral angle at the B3LYP/6-311++G** level of theory. See Section IV.1 of the text. [c] Rotational constants are calculated from B3LYP/6-311++G** geometries using the procedure outlined in Section IV.2.B.

3. Energetics. Table 6 reports AEAs, the position of the most intense peak of the feature A (and a) multiplet (a sort of "vertical EA", vEA), $\tilde{A}$ state term energies (T_0), and calculated V_3 barriers to hindered methyl rotation (eq 7). The AEA of *i*-C_3H_5O is determined as 1.747 ± 0.002 eV, taken from the energy of peak A2 in Figure 7b, compared with the vEA, 1.759 ± 0.002 eV from the position of peak A4. Previous PE and photodetachment studies reported electron affinities of 1.76 ± 0.02[7] and 1.758 ± 0.019 eV,[9] respectively. These previous studies did not resolve any hindered rotor structure of the origin peak, and thus their determinations correspond to our vEA in Table 6. The EA for the *i*-C_3D_5O molecule, 1.743 ± 0.002 eV, is very close to that of its hydrogen analogue. However, the experimental transition that was assigned to the $m_{0a_1;1e}^{0a_1;1e}$ peak in the rotational simulation was the extremely weak peak a2 in Figure 8b, barely visible in the highest resolution scans; the true origin peak could conceivably be buried under baseline noise. Note that the uncertainty reported only includes the peak width of this transition, when visible, and does not reflect any uncertainty in the assignment.

The $\tilde{A}$ state term energy of *i*-methylvinoxy is 1.037 ± 0.002 eV (1.028 ± 0.002 eV for the deuterium compound). As expected, the *i*-C_3H_5O term energy is larger than the previously reported value of 1.01 ± 0.02 eV[7] because our term energy is calculated from the newly resolved 0−0 transition at lower detachment energy. There is a larger difference between term

energies for isotopologues (9 meV) than for EAs (4 meV), indicating that there are differences between the zero-point energies of protonated versus deuterated species. Analogous normal modes in i-C_3H_5O and i-C_3D_5O do not always perfectly match, possibly leading to larger differences between isotope frequencies than might be expected from mass substitution effects alone.

VI. Conclusions

High-resolution SEVI spectra of the *i*-methylvinoxide anions i-$C_3H_5O^-$ and i-$C_3D_5O^-$ are reported. Multiplet structure in the $\tilde{X}\ ^2A'' \leftarrow \tilde{X}\ ^1A'$ spectrum is attributed to hindered rotor motion with the true 0−0 origin peak assigned to one of the smaller peaks below the vEA. This analysis leads to a more accurate i-C_3H_5O EA of 1.747 ± 0.002 eV and T_0 of 1.037 ± 0.002 eV (EA = 1.743 ± 0.002 eV and T_0 = 1.028 ± 0.002 eV for i-C_3D_5O). The presence of hindered rotor transitions in the $\tilde{X}$ state spectra but not the $\tilde{A}$ state spectra supports the lowest-energy geometries determined by electronic structure calculations: the anion $\tilde{X}$ and radical $\tilde{A}$ state have the methyl group in the staggered configuration, whereas the methyl group in the radical $\tilde{X}$ state is eclipsed. Using a 1D model to fit these transitions yields hindered rotor barrier heights of 123 ± 15 and 890 ± 400 cm^{-1} for the ground-state radical and anion, respectively. Vibrational frequencies in the radical $\tilde{X}$ state are assigned on the basis of FC simulations of the $\tilde{X}\ ^2A'' \leftarrow \tilde{X}\ ^1A'$ transition, whereas vibrational assignments of the $\tilde{A}\ ^2A' \leftarrow \tilde{X}\ ^1A'$ transition are proposed by analogy to the $\tilde{X}\ ^2A'' \leftarrow \tilde{X}\ ^1A'$ band.

Acknowledgment. This work was supported by the Air Force Office of Scientific Research under grant nos. F49620-03-1-0085 and FA9550-09-1-0343. T.I.Y. thanks the Fonds Québécois de la Recherche sur la Nature et les Technologies (FQRNT) for a Master's scholarship. T.I.Y. and E.G. thank the National Science and Engineering Research Council of Canada (NSERC) for post graduate scholarships.

References and Notes

(1) Ervin, K. M.; Ho, J.; Lineberger, W. C. *J. Phys. Chem.* **1988**, *92*, 5405.
(2) Müller-Dethlefs, K.; Schlag, E. W. *Angew. Chem., Int. Ed.* **1998**, *37*, 1346.
(3) Cockett, M. C. R. *Chem. Soc. Rev.* **2005**, *34*, 935.
(4) Garand, E.; Zhou, J.; Manolopoulos, D. E.; Alexander, M. H.; Neumark, D. M. *Science* **2008**, *319*, 72.
(5) Hassouna, M.; Delbos, E.; Devolder, P.; Viskolcz, B.; Fittschen, C. *J. Phys. Chem. A* **2006**, *110*, 6667.
(6) Sim, W.-S.; Li, T.-C.; Yang, P.-X.; Yeo, B.-S. *J. Am. Chem. Soc.* **2002**, *124*, 4970.
(7) Alconcel, L. S.; Deyerl, H. J.; Continetti, R. E. *J. Am. Chem. Soc.* **2001**, *123*, 12675.
(8) Zimmerman, A. H.; Reed, K. J.; Brauman, J. I. *J. Am. Chem. Soc.* **1977**, *99*, 7203.
(9) Brinkman, E. A.; Berger, S.; Marks, J.; Brauman, J. I. *J. Chem. Phys.* **1993**, *99*, 7586.
(10) Römer, B. C.; Brauman, J. I. *J. Am. Chem. Soc.* **1997**, *119*, 2054.
(11) Ellison, G. B.; Engelking, P. C.; Lineberger, W. C. *J. Phys. Chem.* **1982**, *86*, 4873.
(12) Williams, S.; Zingher, E.; Weisshaar, J. C. *J. Phys. Chem. A* **1998**, *102*, 2297.
(13) Williams, S.; Harding, L. B.; Stanton, J. F.; Weisshaar, J. C. *J. Phys. Chem. A* **2000**, *104*, 10131.
(14) Yamaguchi, M.; Inomata, S.; Washida, N. *J. Phys. Chem. A* **2006**, *110*, 12419.
(15) Oguchi, T.; Miyoshi, A.; Koshi, M.; Matsui, H.; Washida, N. *J. Phys. Chem. A* **2000**, *105*, 378.
(16) Osterwalder, A.; Nee, M. J.; Zhou, J.; Neumark, D. M. *J. Chem. Phys.* **2004**, *121*, 6317.
(17) Neumark, D. M. *J. Phys. Chem. A* **2008**, *112*, 13287.
(18) Eppink, A.; Parker, D. H. *Rev. Sci. Instrum.* **1997**, *68*, 3477.
(19) Even, U.; Jortner, J.; Noy, D.; Lavie, N.; Cossart-Magos, C. *J. Chem. Phys.* **2000**, *112*, 8068.
(20) Garand, E.; Yacovitch, T. I.; Neumark, D. M. *J. Chem. Phys.* **2009**, *130*, 064304.
(21) Wiley, W. C.; McLaren, I. H. *Rev. Sci. Instrum.* **1955**, *26*, 1150.
(22) Chandler, D. W.; Houston, P. L. *J. Chem. Phys.* **1987**, *87*, 1445.
(23) Sanov, A.; Mabbs, R. *Int. Rev. Phys. Chem* **2008**, *27*, 53.
(24) Hansen, E. W.; Law, P.-L. *J. Opt. Soc. Am. A* **1985**, *2*, 510.
(25) Valli, C.; Blondel, C.; Delsart, C. *Phys. Rev. A* **1999**, *59*, 3809.
(26) Blondel, C. *Phys. Scr.* **1995**, *T58*, 31.
(27) Andersson, M. P.; Uvdal, P. *J. Phys. Chem. A* **2005**, *109*, 2937.
(28) Frisch, M. J.; Trucks, G. W.; Schlegel, H. B.; Scuseria, G. E.; Robb, M. A.; Cheeseman, J. R.; Montgomery, J. A., Jr.; Vreven, T.; Kudin, K. N.; Burant, J. C.; Millam, J. M.; Iyengar, S. S.; Tomasi, J.; Barone, V.; Mennucci, B.; Cossi, M.; Scalmani, G.; Rega, N.; Petersson, G. A.; Nakatsuji, H.; Hada, M.; Ehara, M.; Toyota, K.; Fukuda, R.; Hasegawa, J.; Ishida, M.; Nakajima, T.; Honda, Y.; Kitao, O.; Nakai, H.; Klene, M.; Li, X.; Knox, J. E.; Hratchian, H. P.; Cross, J. B.; Adamo, C.; Jaramillo, J.; Gomperts, R.; Stratmann, R. E.; Yazyev, O.; Austin, A. J.; Cammi, R.; Pomelli, C.; Ochterski, J. W.; Ayala, P. Y.; Morokuma, K.; Voth, G. A.; Salvador, P.; Dannenberg, J. J.; Zakrzewski, V. G.; Dapprich, S.; Daniels, A. D.; Strain, M. C.; Farkas, O.; Malick, D. K.; Rabuck, A. D.; Raghavachari, K.; Foresman, J. B.; Ortiz, J. V.; Cui, Q.; Baboul, A. G.; Clifford, S.; Cioslowski, J.; Stefanov, B. B.; Liu, G.; Liashenko, A.; Piskorz, P.; Komaromi, I.; Martin, R. L.; Fox, D. J.; Keith, T.; Al-Laham, M. A.; Peng, C. Y.; Nanayakkara, A.; Challacombe, M.; Gill, P. M. W.; Johnson, B.; Chen, W.; Wong, M. W.; Gonzalez, C.; Pople, J. A. *Gaussian 03*, revision C.02; Gaussian, Inc.: Wallingford, CT, 2004.
(29) Duschinsky, F. *Acta Physicochim. URSS* **1937**, *7*, 551.
(30) Metz, R. B.; Cyr, D. R.; Neumark, D. M. *J. Phys. Chem.* **1991**, *95*, 2900.
(31) Adams, C. L.; Schneider, H.; Ervin, K. M.; Weber, J. M. *J. Chem. Phys.* **2009**, *130*, 074307.
(32) Ervin, K. M. *FCFGAUS03: Gaussian 03 Output Conversion Program*, 2009.
(33) Ervin, K. M. *PESCAL, Fortran program*, 2009.
(34) Chen, P. Photoelectron Spectroscopy of Reactive Intermediates. In *Unimolecular and Bimolecular Reaction Dynamics*; Baer, T., Ng, C.-Y., Powis, I., Eds.; John Wiley & Sons: Chichester, U.K., 1994; pp 371−425.
(35) Pitzer, K. S.; Gwinn, W. D. *J. Chem. Phys.* **1942**, *10*, 428.
(36) Pitzer, K. S. *J. Chem. Phys.* **1946**, *14*, 239.
(37) Kilpatrick, J. E.; Pitzer, K. S. *J. Chem. Phys.* **1949**, *17*, 1064.
(38) Bunker, P. R.; Jensen, P. *Molecular Symmetry and Spectroscopy*, 2nd ed.; NRC Research Press: Ottawa, 1998.
(39) Wigner, E. P. *Phys. Rev.* **1948**, *73*, 1002.
(40) Yacovitch, T. I.; Garand, E.; Neumark, D. M. *J. Chem. Phys.* **2009**, *130*, 244309.
(41) Alconcel, L. S.; Deyerl, H. J.; Zengin, V.; Continetti, R. E. *J. Phys. Chem. A* **1999**, *103*, 9190.
(42) Brock, L. R.; Rohlfing, E. A. *J. Chem. Phys.* **1997**, *106*, 10048.

JP101930B